Research Article | Vol. 28, No. 23 / 9 November 2020 / Optics Express 34606
Optics EXPRESS

Impact of angular pointing error on BER performance of underwater optical wireless links

RUBÉN BOLUDA-RUIZ,[1,*] ANTONIO GARCÍA-ZAMBRANA,[1] BEATRIZ CASTILLO-VÁZQUEZ,[1] AND STEVE HRANILOVIC[2]

[1]Dept. of Communications Engineering, Andalucía Tech, University of Málaga, Málaga E-29071, Spain
[2]Dept. of Electrical and Computer Engineering, McMaster University, Hamilton, Ontario, Canada
[*]rbr@ic.uma.es

Abstract: Even in clear ocean water, underwater optical wireless communication (UOWC) is impaired not only by absorption and scattering, but also by oceanic turbulence and dynamic pointing errors which result in a fading channel, degrading the bit error rate (BER) performance. In this paper, for the first time, we quantify analytically the trade-off between geometric loss and misalignment in underwater scattering channels. A novel geometric loss model is developed which is used to compute the average BER in the presence of absorption and scattering over salinity-induced oceanic turbulence channels. Our findings suggest that UOWC systems are less sensitive to angular pointing errors due to jitter since scattering is able to alleviate such a fading effect at the expense of a higher attenuation due to geometric spread. Monte Carlo simulation results are further included to verify the developed BER expression which is valid over a wide range of signal-to-noise-ratio (SNR). Finally, the impact of inter-symbol interference (ISI) is also quantified by measuring the optical power penalty.

1. Introduction

Researchers worldwide are developing high-speed and long-distance underwater wireless links due to the increasing need to explore the oceans for a great deal of scientific and industrial activities, as well as for military operations. Within this context, the need for transmitting large amounts of data has become vital [1]. Underwater optical wireless communication (UOWC) systems, using the blue-green band of the visible spectrum, are able to meet this technological demand by promising a high bandwidth and low latency compared to acoustic and radio-frequency (RF) systems [2]. However, in addition to absorption, the transmission of wireless optical signals through seawater is mainly impaired by the level of turbidity of the water, resulting in signal scattering that can limit the achievable performance [3]. Scattering can lead to an important temporal dispersion that results in inter-symbol interference (ISI) by changing the direction of the transmitted photons. In the last decade, special attention has been paid to underwater optical channel modeling [4–7] (and references therein), where different solutions are presented, both numerical and analytical, to describe the underwater channel by means of channel impulse response (CIR) and channel path loss. Despite the fact that scattering is the major impairment, new findings have revealed that the performance of UOWC systems can be also affected by oceanic turbulence and misalignment errors. Oceanic turbulence, though considered to be less of an issue [4], is commonly caused by small variations in salinity, temperature, pressure and air bubbles, resulting in signal fading that causes fluctuations in the irradiance of the transmitted optical beam [1,2]. On the other hand, although UOWC systems are deployed for moderate distances (10-100 m) due to scattering, in practice, there will likely be some pointing mismatch between UOWC transceivers even in clear water conditions. Autonomous underwater vehicles (AUVs) and remotely operated vehicles (ROVs) have become useful devices for ocean exploration

#405942 https://doi.org/10.1364/OE.405942
Journal © 2020 Received 21 Aug 2020; revised 1 Oct 2020; accepted 13 Oct 2020; published 29 Oct 2020

Optics EXPRESS

and data collection. Under severe sea conditions, the destabilizing effect of ocean and tidal currents on AUVs and ROVs is one of the limiting factors in spite of having position and attitude control systems [8–10]. Due to the fact that there is a limit to the ability of these devices to stabilize, the presence of internal currents that are very often generated in the ocean, resulting in water flows [11], as well as random sea surface slopes [12] can still cause misalignments in these systems due to jitter, leading to an important communication loss problem. Some authors have studied numerically the impact of off-axis received power on different types of water by Monte Carlo methods [13–15]. It was concluded that under highly scattering conditions such as harbor water, the effect of misalignment is mitigated due to the optical beam spreading, but reducing severely the intensity of the received signal. On the contrary, a significant power reduction is observed in clear ocean and coastal waters. This leads us to intuit that a misalignment error will result in a significant random fading that will considerably degrade the performance of such systems. Thus, more study is required to understand with greater detail how the combined effect of oceanic turbulence and angular pointing errors in the presence of absorption and scattering might limit the maximum achievable performance.

Although the study of some of these impairments in UOWC systems has been addressed in the literature, to the best of the authors' knowledge, there is limited work that has considered their combined impact [16–25] (and references therein). However, such a model is essential to enable a complete system design for UOWC systems. In [16], the bit-error rate (BER) performance of single-input/multiple-output (SIMO) UOWC systems in the presence of log-normal (LN) oceanic turbulence without considering pointing errors is analyzed when the effect of scattering is not so significant. The BER performance of multi-hop [17] and multiple-input/multiple-output (MIMO) UOWC systems [18] is computed over LN oceanic turbulence channels with no pointing errors where temporal dispersion produced by scattering is taken into account. In [19], the BER performance is evaluated for inhomogeneous underwater links in the absence of oceanic turbulence and pointing errors. In [20], the upper bound of the average BER is obtained for pulse position modulated (PPM) operating in weak oceanic turbulence. In [21,22], the BER performance in the presence of salinity-induced oceanic turbulence modeled by Weibull distributions is analyzed when scattering and pointing errors effects are neglected. In [23], the BER performance of UOWC systems is investigated over weak oceanic turbulence by employing binary phase shift keying-subcarrier intensity modulation (BPSK-SIM). In [24], the BER performance over weak oceanic turbulence channels with no pointing errors is conducted when employing orthogonal frequency-division multiplexing (OFDM). In [25], the ergodic capacity of UOWC systems is evaluated over Málaga oceanic turbulence channels in the absence of pointing errors. In these studies, as can be noted, the temporal dispersion produced by scattering is usually ignored when analyzing the performance of UOWC systems. Such a temporal dispersion should be considered when designing high-speed links since it limits the maximum data rate.

On the other hand, the effect of potential pointing errors (jitter) between transmitter and receiver is also neglected for simplicity. Unlike terrestrial free-space optical systems, UOWC transceivers do not have to be at the same distance from both the sea surface and marine soil, enabling both horizontal and vertical links. This specific feature makes the received optical beam be non-orthogonal in general with respect to the detector plane. Thus, this pointing error is termed here as angular pointing error. In addition to this, as a direct consequence of not being perfectly aligned, these links will be surely affected by a nonzero boresight displacement which requires additional consideration. Recently, some authors have analyzed the BER performance of UOWC systems under pointing error effects [26–28]. They used a geometrical loss model for laser beam transmission that is shown to be inaccurate where the beamwidth expansion due to scattering is not taken into account and, hence, underestimating the achievable BER performance.

In this paper, we develop a new closed-form expression for the BER of UOWC systems in the presence of absorption and scattering over salinity-induced oceanic turbulence channels with

Optics EXPRESS

angular pointing errors. The temporal dispersion caused by scattering is included in terms of the CIR in order to make this BER performance analysis closer to realistic UOWC scenarios. The Weibull oceanic turbulence model has been adopted due to the fact that salinity gradient is present in the open water, lakes, seas, and oceans of the world where most of the potential applications related to ocean observation and military operations, among others, take place. It was demonstrated that this oceanic turbulence model fits very well with the experimental data in many channel conditions [29,30]. Adaptive optics correction techniques for optical beams affected by salinity-induced oceanic turbulence have been also investigated [31]. Unlike [26–28], we further compute angular pointing errors with nonzero boresight displacements by quantifying analytically the trade-off between geometric loss and misalignment for laser beam transmission in the presence of scattering, so that the whole received power is considered. Thus, the developed geometric loss model is used to evaluate the BER over a wide range of signal-to-noise-ratio (SNR) for clear ocean and coastal waters. In order to get further insights, a new asymptotic BER expression is also derived at high SNR which is used to compute the optical power penalty (OPP) induced by ISI. Our results confirm that the BER performance of UOWC systems is drastically impacted by angular pointing errors due to jitter. However, scattering offers a natural mechanism to mitigate such a fading effect. Monte Carlo simulation results are included to verify the analytical results.

The remainder of this paper is organized as follows. The system model is outlined in Section 2, and the UOWC channel model is described statistically in Section 3. In Section 4, we conduct the BER performance analysis in the presence of absorption and scattering, salinity-induced oceanic turbulence and angular pointing errors. In Section 5, some practical examples are illustrated to show the validity of the developed BER expressions. Finally, Section 6 concludes the paper.

2. System model

Consider a UOWC link using on-off keying (OOK) modulation where a symbol-by-symbol detection is assumed. The BER for this UOWC system based on intensity-modulation/direct-detection (IM/DD) is computed as in [32, Chapter 6] as follows. We denote that y_k, the input to the decision device at the receiver, is expressed as

$$y_k = 2RP_t\sqrt{T_b\xi}\cdot h\cdot a_k * p_k + z_k, \tag{1}$$

where R is the detector responsivity, P_t is the average transmitted optical power, T_b is the bit period, h is the fading coefficient, ξ is related to the pulse shape, $a_k \in \{0,1\}$ are the symbols to be transmitted, the symbol * denotes convolution, and p_k is the equivalent discrete-time impulse response of the system given by

$$p_k = p(kT_b) = g(t) * \mathrm{CIR}(t) * f(t)|_{t=kT_b}, \tag{2}$$

where $\mathrm{CIR}(t)$ is the normalized fading-free channel impulse response obtained in [7, Eq. (8)] that models the temporal dispersion caused by scattering, $g(t)$ is the transmitter filter, and $f(t)$ is the receiver filter that is matched to $g(t)$, i.e, $f(t) = g(-t)$. We assume a simple OOK system, so that $g(t)$ is a rectangular pulse with normalized amplitude of duration κT_b, being κ the duty cycle. For instance, when using a rectangular pulse shape of duration κT_b with $\kappa \in (0,1]$, a value of $\xi = 1/\kappa$ is obtained [33]. For non-return zero (NRZ) OOK systems, $g(t)$ and $f(t)$ are identical rectangular pulses of duration T_b, i.e. a 100% duty cycle. Finally, z_k is obtained as follows

$$z_k = z(kT_b) = n(t) * f(t)|_{t=kT_b}, \tag{3}$$

where $n(t)$ is additive white Gaussian noise (AWGN) with zero mean and variance $N_0/2$. Owing to the fact that the different noise sources are additive and independent from each other, they are

Optics EXPRESS

statistically modeled as a Gaussian distribution. For the sake of simplicity, we assume that the effect of deep sea, as well as potential beam blockage due to bubbles and/or other particles are beyond the scope of this paper.

3. Channel model

The UOWC fading coefficient, h, is defined as a product of three factors given by $h = L \cdot h_o \cdot h_{ap}$, where L is the oceanic path loss, h_o is the salinity-induced oceanic turbulence, and h_{ap} are the geometric spread and angular pointing errors.

3.1. Oceanic path loss

The oceanic path loss, L, is determined by the exponential Beers-Lambert law as

$$L = \exp(-F \cdot c_T \cdot d), \tag{4}$$

where d is the UOWC link distance, $c_T(\lambda) = c_1(\lambda) + c_2(\lambda)$ $[m^{-1}]$ is the extinction coefficient described in [3] (c_1 and c_2 represent absorption and scattering, respectively), and F is a coefficient that is computed via data fitting to simulation data that models the increase in received power due to scattering [7]. Here, the values of $c_1(\lambda)$ and $c_2(\lambda)$ for clear ocean and coastal waters are outlined in Table 1 for a value of wavelength of 532 nm.

Table 1. Extinction coefficient.

Water type	$c_1[m^{-1}]$	$c_2[m^{-1}]$	$c_T[m^{-1}]$
Clear ocean water	0.114	0.037	0.151
Coastal water	0.179	0.219	0.398

3.2. Salinity-induced oceanic turbulence

The probability density function (PDF) associated with salinity-induced oceanic turbulence is modeled as a Weibull distribution as

$$f_{h_o}(h) = \frac{\beta_1}{\beta_2}\left(\frac{h}{\beta_2}\right)^{\beta_1 - 1} \times e^{-\left(\frac{h}{\beta_2}\right)^{\beta_1}}, \quad h \geq 0, \tag{5}$$

where $\beta_1 > 0$ is the shape parameter related to the scintillation index, and $\beta_2 > 0$ is the scale parameter related to the mean value of oceanic turbulence. By fitting such a turbulence model to simulated or experimental PDF data, some expressions for β_1 and β_2 have been developed in [30]. The scintillation index, $\sigma_{h_o}^2$, is defined in terms of the Weibull parameters as

$$\sigma_{h_o}^2 = \frac{\mathbb{E}[h_o^2] - \mathbb{E}[h_o]^2}{\mathbb{E}[h_o]^2} = \frac{\Gamma\left(1 + 2/\beta_1\right)}{\Gamma\left(1 + 1/\beta_1\right)^2} - 1, \tag{6}$$

where $\mathbb{E}[\cdot]$ denotes expectation, and $\Gamma(\cdot)$ is the well-known Gamma function [34, Eq. (8.310)]. Under the assumption that weak and moderate oceanic turbulence conditions, β_1 can be well approximated by

$$\beta_1 \simeq \left(\sigma_{h_o}^2\right)^{-6/11}. \tag{7}$$

As explored in Appendix A, the above scintillation index can be expressed as a function of distance as

$$\sigma_{h_o}^2(d) \simeq \lambda_1 d^2 + \lambda_2 d + \lambda_3, \quad d \leq 100 \text{ m}. \tag{8}$$

Finally, assuming $\mathbb{E}[h_o] = \beta_2 \Gamma\left(1 + 1/\beta_1\right) = 1$, β_2 can be expressed as

$$\beta_2 = 1/\Gamma\left(1 + 1/\beta_1\right). \tag{9}$$

Optics EXPRESS

3.3. Angular pointing errors

As shown in Appendix B, the attenuation due to geometric spread at the receiver with pointing error r for a laser source with a Gaussian beam shape in the presence of scattering can be well approximated as

$$h_{ap}(r) \simeq k_1 A_0 \exp\left(-2r^2/\omega_{z_{eq}}^2\right), \tag{10}$$

where $\omega_{z_{eq}}^2 = \omega_z^2(k_2)\sqrt{\pi}\mathrm{erf}(v)/2v\exp(-v^2)$ is the equivalent beamwidth, $A_0 = [\mathrm{erf}(v)]^2$ is the fraction of the collected power at $r = 0$, $v = \sqrt{\pi}\sqrt{a\rho}/\sqrt{2}\omega_z$, a is the receiver aperture radius, and $\rho = a\cos\theta\cos\phi$ is the parameter that determines the power reduction due to an angular misalignment. As commented in the introduction, the optical beam may not be orthogonal on the photodetector plane, as shown in Fig. 1. This means that the fraction of the power captured at the receiver is not calculated by the area of a circular receiver aperture, but also by the area of a rotated ellipse that is calculated by the angles θ and ϕ in xy-plane, as demonstrated in [35,36], being z the transverse axis. Finally, the beamwidth at the receiver plane, $\omega_z(k_2)$, can be approximated as

$$\omega_z(k_2) \simeq k_2 \cdot \theta_0 \cdot d, \tag{11}$$

where k_1 and k_2 are the coefficients that are obtained via data fitting to simulation data to model the increase in beam spreading due to scattering, and θ_0 is the divergence angle at $1/e$. Note that the above approximation, which is verified by Monte Carlo simulations in Appendix B for clear ocean and coastal waters, does not underestimate the true received power due to scattering. As an added feature, the above approximation is even consistent with non-dispersive media, i.e. when $c_2 = 0$, by setting $k_1 = k_2 = 1$ [37].

As commented in Section 1, UOWC transceivers are strongly affected by ocean currents and other disturbances which result in changes of their position and attitude. This leads to a misalignment error between them. Without loss of generality, we model such a misalignment error as a radial displacement at the detector plane as $r^2 = x^2 + y^2$ where x (horizontal displacement) and y (elevation) are modeled as independent Gaussian distributions, i.e., $x \sim N(\mu_x, \sigma_x)$ and $y \sim N(\mu_y, \sigma_y)$, respectively. Thus, the pointing error r is randomized according to the Beckmann distribution [38, Eq. (31)] whose PDF can be well approximated by a modified Rayleigh distribution as in [39, Eq. (11)] as follows

$$f_r(r) = \frac{r}{2\pi\sigma_x\sigma_y}\int_0^{2\pi}\exp\left(-\frac{(r\cos\theta-\mu_x)^2}{2\sigma_x^2} - \frac{(r\sin\theta-\mu_y)^2}{2\sigma_y^2}\right)d\theta \simeq \frac{r}{\sigma_{ap}^2}\exp\left(-\frac{r^2}{2\sigma_{ap}^2}\right), \tag{12}$$

where σ_{ap}^2 is given by [39, Eq. (9)] as

$$\sigma_{ap}^2 = \left(3\mu_x^2\sigma_x^4 + 3\mu_y^2\sigma_y^4 + \sigma_x^6 + \sigma_y^6/2\right)^{1/3}. \tag{13}$$

Thus, combining Eqs. (10), (11) and (12), the PDF of the angular pointing error is given by

$$f_{h_{ap}}(h) \simeq \frac{\varphi_{ap}^2}{A_{ap}^{\varphi_{ap}^2}} h^{\varphi_{ap}^2-1}, \quad 0 \le h \le A_{ap}, \tag{14}$$

where $\varphi_{ap} = \omega_{z_{eq}}/2\sigma_{ap}$, and A_{ap} was obtained in [39] as

$$A_{ap} = k_1 A_0 \exp\left(\frac{1}{\varphi_{ap}^2} - \frac{1}{2\varphi_x^2} - \frac{1}{2\varphi_y^2} - \frac{\mu_x^2}{2\sigma_x^2\varphi_x^2} - \frac{\mu_y^2}{2\sigma_y^2\varphi_y^2}\right), \tag{15}$$

where $\varphi_x = \omega_{z_{eq}}/2\sigma_x$ and $\varphi_y = \omega_{z_{eq}}/2\sigma_y$. Despite the fact that the PDF in Eq. (14) presents the same mathematical appearance as previous pointing error modeling already reported for

Optics EXPRESS

non-dispersive channels, this PDF includes the new parameters k_1 and k_2 to model geometric loss in the presence of scattering for clear ocean and coastal waters. This model will be used to evaluate the BER performance of UOWC systems in the next section.

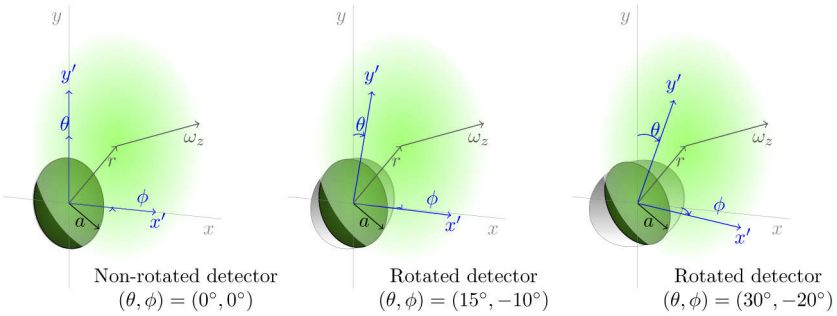

Fig. 1. Beam footprint with angular pointing errors on different circular detectors of radius a. The angles θ and ϕ model the orientation of each detector in x-axis and y-axis, respectively. Each detector is depicted in gray color, and the effective capture area of each detector is depicted in dark green. In the first diagram, the power captured at the non-rotated detector is computed by the area of a circle. However, in the other diagrams, the power captured at the rotated detectors is computed by the area of an ellipse in the xy-plane. Due to the pointing error r, a fraction of such an effective capture area does not collect power.

3.4. Composite fading channel

The PDF of the channel $h = L \cdot h_o \cdot h_{ap}$ is written as follows

$$f_h(h) = \int_{h/A_{ap}L}^{\infty} f_{h|h_o}(h|h_o) f_{h_o}(h_o) dh_o. \tag{16}$$

The above integral can be expressed in terms of an upper incomplete Gamma function $\Gamma(\cdot,\cdot)$ [40, Eq. (6.5.3)], yielding

$$f_h(h) = \frac{\varphi_{ap}^2}{\left(A_{ap}L\beta_2\right)^{\varphi_{ap}^2}} h^{\varphi_{ap}^2-1} \Gamma\left(1 - \frac{\varphi_{ap}^2}{\beta_1}, \left(\frac{h}{A_{ap}L\beta_2}\right)^{\beta_1}\right), \quad h \geq 0. \tag{17}$$

4. BER performance analysis

The performance of UOWC systems in terms of the BER is analyzed. Under the assumption that channel state information (CSI) is available at the receiver, the conditional BER for the UOWC system under study is given by

$$P_b = Q\left(\sqrt{2\gamma\xi\left(1 - X_k\right)^2} \cdot h\right), \tag{18}$$

where $Q(\cdot)$ is the Gaussian-Q function, $\gamma = P_t^2 T_b / N_0$ represents the normalized received electrical SNR in the absence of fading, and $X_k = 2\sum_{n\neq k} a_n p_{k-n}$ represents the ISI. In practice, ISI only affects to a finite number of symbols and, hence, the summation can be performed over all $a_k \in \{0,1\}^M$, where M is the length of the channel impulse response tail. Moreover, the UOWC channel is considered to be slow [30], so that the fading coefficient h can be assumed to be fixed and easily estimated at the receiver during the transmission of the bit a_k and also during the

Optics EXPRESS

transmission of all the interfering bits a_n for all $n \neq k$ causing ISI to a_k. Then, the total BER is derived by averaging over h and all possible bit sequences as follows

$$P_b = \frac{1}{2^M} \sum_{a_k} \int_0^\infty Q\left(\sqrt{2\gamma\xi \left(1 - X_k\right)^2} \cdot h\right) f_h(h) dh. \tag{19}$$

To solve the above integral, we firstly use the relation between the Q-function and $\mathrm{erfc}(\cdot)$ by $\mathrm{erfc}(x) = 2Q(\sqrt{2}x)$ [34, Eq. (6.287)]. Then, we can use the fact that both $\mathrm{erfc}(\cdot)$ and $\Gamma(\cdot,\cdot)$ can be expressed in terms of the Meijer's G-function $G_{p,q}^{m,n}[\cdot]$ [34, Eq. (7.811)] as $\mathrm{erfc}(\sqrt{z}) = (1/\sqrt{\pi}) G_{1,2}^{2,0}\left[z|_{0,1/2}^{1}\right]$ [41, Eq. (06.27.26.0006.01)] and $\Gamma(a,z) = G_{1,2}^{2,0}\left[z|_{0,a}^{1}\right]$ [41, Eq. (06.06.26.0005.01)], respectively. Finally, a closed-form expression for the BER of the UOWC system under study is expressed in terms of the H-Fox function $H_{p,q}^{m,n}[\cdot]$ [42, Eq. (1.1)] as follows

$$P_b \simeq \frac{1}{2^M} \frac{\varphi_{ap}^2}{2\beta_2\sqrt{\pi}} \sum_{a_k} H_{3,3}^{2,2}\left[(\gamma\xi)\left(A_{ap} L \beta_2\right)^2 \left(1 - X_k\right)^2 \middle| \begin{matrix} \left(1 - \frac{\varphi_{ap}^2}{\beta_1}, \frac{2}{\beta_1}\right), \left(0, \frac{2}{\beta_1}\right), (1,1) \\ \left(\frac{1}{2}, 1\right), (0,1), \left(-\frac{\varphi_{ap}^2}{\beta_1}, \frac{2}{\beta_1}\right) \end{matrix} \right]. \tag{20}$$

In order to get further insights, we consider the asymptotic BER performance at high SNR to provide a tool to understand the dominant factors impacting on BER. Thus, the BER at high SNR tends to $P_b \doteq (G_c \gamma\xi)^{-G_d}$ [39,43], where G_d represents the diversity order and G_c the coding gain. To do that, we can approximate the PDF of h by a single polynomial term as $f_h(h) \doteq m_1 h^{m_2 - 1}$ [39,43] using the series expansion of $\Gamma(\cdot,\cdot)$ [40, Eq. (8.354.2)] as follows

$$f_h(h) \doteq m_1 h^{m_2-1} = \begin{cases} \frac{\varphi_{ap}^2 \beta_1}{\left(A_{ap} L \beta_2\right)^{\beta_1} \left(\varphi_{ap}^2 - \beta_1\right)} h^{\beta_1 - 1}, & \varphi_{ap}^2 > \beta_1, \\ \frac{\varphi_{ap}^2 \Gamma\left(1 - \frac{\varphi_{ap}^2}{\beta_1}\right)}{\left(A_{ap} L \beta_2\right)^{\varphi_{ap}^2}} h^{\varphi_{ap}^2 - 1}, & \varphi_{ap}^2 < \beta_1. \end{cases} \tag{21}$$

Substituting Eq. (21) into Eq. (19) and, making use of $\int_0^\infty \mathrm{erfc}(cx) x^{\alpha-1} e^{-px} dx$ [44, Eq. (2.8.5.2)], the corresponding asymptotic solution for the BER can be expressed as

$$\begin{aligned} P_b \doteq & \frac{1}{2^M} \sum_{a_k} \frac{\varphi_{ap}^2 \Gamma\left(\left(\beta_1 + 1\right)/2\right) \left(1 - X_k\right)^{-\beta_1}}{2\sqrt{\pi} \left(A_{ap} L \beta_2\right)^{\beta_1} \left(\varphi_{ap}^2 - \beta_1\right)} (\gamma\xi)^{-\beta_1/2} \\ & + \frac{1}{2^M} \sum_{a_k} \frac{\Gamma\left(\left(\varphi_{ap}^2 + 1\right)/2\right) \Gamma\left(1 - \frac{\varphi_{ap}^2}{\beta_1}\right)}{2\sqrt{\pi} \left(A_{ap} L \beta_2\right)^{\varphi_{ap}^2} \left(1 - X_k\right)^{\varphi_{ap}^2}} (\gamma\xi)^{-\varphi_{ap}^2/2}. \end{aligned} \tag{22}$$

As we can observe from such an asymptotic expression, the diversity order is easily obtained as

$$G_d = m_2/2 = \min\left(\beta_1, \varphi_{ap}^2\right)/2. \tag{23}$$

Note that above expression is useful since we can determine when oceanic turbulence or angular pointing errors result in being dominant at high SNR. Two different UOWC scenarios can be analyzed depending on the relationship $\beta_1 < \varphi_{ap}^2$ is satisfied or not. When this condition holds, oceanic turbulence is dominating the average BER at high SNR. Based on this, a higher diversity order, which is computed by $\beta_1/2$, is achieved. In other words, the diversity order depends only on oceanic turbulence, while the coding gain is affected by angular pointing errors and ISI. On the contrary, when $\beta_1 < \varphi_{ap}^2$ does not hold, the diversity order is determined by $\varphi_{ap}^2/2$, i.e., by angular pointing errors.

Optics EXPRESS

5. Results and discussion

In this section, the average BER of UOWC systems is computed via Eqs. (20) and (22) for clear ocean and coastal waters and verified by Monte-Carlo simulations. Without loss of generality, the BER performance for oceanic path loss of $L = 1$ is computed. For simulation purposes, the main UOWC system parameters considered here are outlined in Table 2 where UOWC link distances of $d = \{30, 40, 50\}$ m and $d = \{15, 25, 35\}$ m are assumed for clear ocean and coastal waters, respectively, as well as a transmit divergence angle of $\theta_0 = 10$ mrad is assumed. A data rate $R_b = 1$ Gbps is used which is feasible given the experiments already reported to get long-distance and high-speed underwater links by using LDs in the blue-green band [45–47]. Data rate values of 2.2 Gbps, 2.7 Gbps and 2.5 Gbps are reported at distances of 12 m, 35.5 m and 60 m, respectively, when employing NRZ OOK modulation. Additionally, a commercial UOWC system (BlueComm-200) is available to use for an optical communication range up to 150 m [48]. Also, note that the normalized fading-free channel impulse response, CIR(t), is obtained via Monte Carlo simulation, as described in [7], by sending 10^9 photons and simulating their interaction with the medium where the Henyey-Greenstein phase function was utilized as the angular distribution of scattering in water. Here, β_1 and β_2 are computed from Eqs. (7) and (9) for salinity-induced oceanic turbulence assuming plane wave propagation when the relative strength of temperature and salinity fluctuations is equal to $w = -1$ [49,50]. For the sake of simplicity, the BER performance is evaluated for the same jitter variances, i.e., $\sigma_x = \sigma_y = \sigma_s$. In this way, normalized jitter values of $\sigma_s/a = \{1, 2\}$ are used to emulate different severity of pointing errors. A nonzero boresight error of $s/a = 1$ is assumed when the normalized rotation parameter takes values of $\rho/a = \{0.8, 0.9\}$ to evaluate angular misalignment. Finally, the parameters k_1 and k_2 required to compute the attenuation due to geometric spread from Eq. (10) are summarized in Table 4 in Appendix B for different distances.

Table 2. Major UOWC system parameters.

Parameter	Symbol	Value
Wavelength	λ	532 nm
Responsivity	R	1
Rectangular pulse shape with a 100% duty cycle	ξ	1
LD divergence angle at $1/e$	θ_0	10 mrad
Receiver aperture diameter	$D = 2a$	20 cm
Receiver field-of-view (FOV)	FOV	180°
Relative strength of temperature and salinity fluctuations	w	-1
Beamwidth at the receiver plane	ω_z	$\simeq k_2 \cdot \theta_0 \cdot d$
Normalized standard deviation (jitter)	σ_s/a	$\{1, 2\}$
Normalized boresight displacement	s/a	1
Normalized rotation parameter	ρ/a	$\{0.8, 0.9\}$

5.1. BER results

In Figs. 2(a) and 2(b), the average BER is depicted as a function of the electrical SNR γ[dB] for clear ocean and coastal waters, respectively. Note that the electrical SNR represents the square of the optical SNR since it depends on the square of the received optical power when employing IM/DD systems. In general, it is observed that the BER closed-form expressions obtained in Eqs. (20) and (22) are in good agreement with the Monte Carlo simulation results.

Optics EXPRESS

On the one hand, it is verified that the BER performance is strongly dependent on the attenuation length $\tau = c_T \cdot d$, degrading such a performance as the UOWC link distance slightly increases and/or the effect of scattering becomes significant. On the other hand, it is seen that the effect of oceanic turbulence modeled by Weibull distributions cannot be ignored when evaluating the performance of real UOWC systems, particularly in open waters. In addition, the strength of such a turbulence-induced fading becomes more important when link distance increases, decreasing the diversity order and limiting the maximum achievable distance for potential applications.

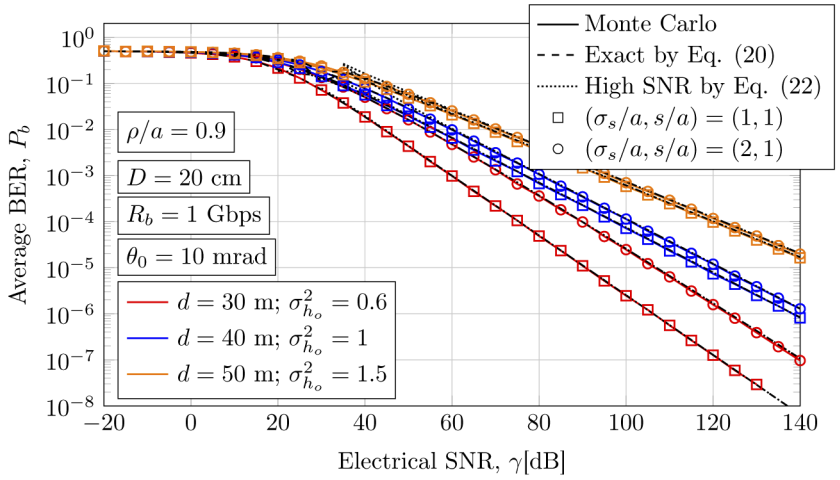

(a) Clear ocean water

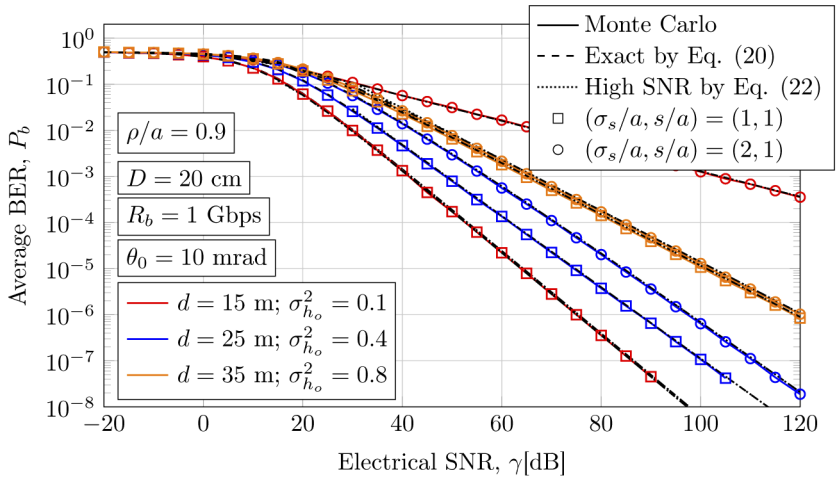

(b) Coastal water

Fig. 2. Average BER performance for (a) clear ocean, and (b) coastal waters over salinity-induced oceanic turbulence in the presence of angular pointing errors when a receiver aperture diameter of $D = 20$ cm and a value of FOV = 180° are considered. These BER results correspond to a UOWC system using NRZ OOK modulation when the data rate is equal to $R_b = 1$ Gbps.

According to simulations, given the physical characteristics of the laser source used in this paper, the effect of ISI due to temporal dispersion can be considered as negligible in this type of water as we can see in Fig. 2(a), resulting in a quasi-flat channel that allows to deploy longer

Optics EXPRESS

point-to-point communication link as required in ocean observation. In other words, the effect of ISI is not significant when increasing the data rate in this scenario. ISI might be a serious issue for much higher data rates. The length of the channel impulse response tail is equal to $M = 1$ in this figure which also verifies that temporal dispersion is not so relevant. Different results would be obtained when employing light emitting diodes (LEDs) with Lambertian emission as a transmitter source since the optical beam would spread even more as distance increases. Similar conclusions were obtained in [4] when studying channel impulse response.

Regarding the impact of angular pointing errors, it can be observed that for 40 and 50 m UOWC link distances, an increase in jitter severity, i.e. when $\sigma_s/a = 2$, does not result in excessive performance degradation since the beamwidth is large enough with respect to the radius of the receiver aperture to mitigate the effect of jitter. The normalized beamwidth is even lager in the presence of scattering, making the laser beam spread even more, as can be seen in Appendix B. This leads to a natural mechanism to mitigate potential angular pointing errors due to jitter at the expense of a higher attenuation due to geometric spread. This physical feature has not been revealed in early paper when studying the performance of UOWC systems under pointing error effects [26–28]. It is also observed that for a UOWC link distance of 30 m, the impact of jitter severity is major in comparison with the rest of link distances considered. In other words, the relative impact of jitter severity on the BER performance becomes less important as link distance increases. The reason behind this is that the normalized beamwidth at the receiver plane is not large enough to mitigate the effect of jitter due to the fact that the distance is relatively short. Even so, the BER slope at high SNR is still dominated by oceanic turbulence for the whole set of link distances considered in Fig. 2(a) and not by angular pointing errors, i.e, $G_d = \beta_1/2$.

In Fig. 2(b), the same conclusions as in the previous subfigure can be drawn from a general viewpoint. However, due to the fact that the effect of scattering is even more significant in coastal water than in clear ocean water, potential UOWC systems would be deployed for shorter communication link distances in order to provide a good BER performance. Interestingly, the BER performance gets much worse when the jitter severity increases for a UOWC link distance of 15 m. Unlike the cases of 25 and 35 m, the BER slope at high SNR is now dominated by angular pointing errors and not by oceanic turbulence, i.e, $G_d = \varphi_{ap}^2/2$. This is due to the fact that the beamwidth at the receiver plane is not large enough to mitigate the jitter effect. The length of the channel impulse response tail in this figure takes values of $M = \{2, 3\}$, depending on distance. In Fig. 3, the average BER is plotted as a function of the electrical SNR γ[dB] for coastal water. Here, pointing errors values of $(\sigma_s/a, s/a) = (2, 1)$, and a normalized rotation parameter value of $\rho/a = 0.8$ are assumed. In this figure, we graphically depict the impact of ISI on the BER performance due to temporal dispersion caused by scattering when the data rate is set to $R_b = \{0.1, 1, 2\}$ Gbps for a UOWC link distance of $d = 35$ m (labeled with PE). It is important to note that when the data rate increases, the effect of ISI starts to become significant by inducing a considerable power penalty in decibels that depends on the UOWC system parameters. It is evident that the channel impulse response in UOWC systems must be included in the analysis since it presents a remarkable impact in terms of reliable communications system design. As a reference, the BER performance for an ideal AWGN channel (labeled AWGN), as well as when no angular pointing errors are considered (labeled no PE) are also plotted.

5.2. Optical power penalty (OPP) results

For a better understanding of the impact of ISI on the BER performance of UOWC systems, we obtain the OPP[dB] when oceanic turbulence is the dominant effect at high SNR, since it achieves higher diversity gains under this condition. We quantify the OPP[dB] between the BER when temporal dispersion produced by scattering is neglected and the BER when such a temporal

Optics EXPRESS

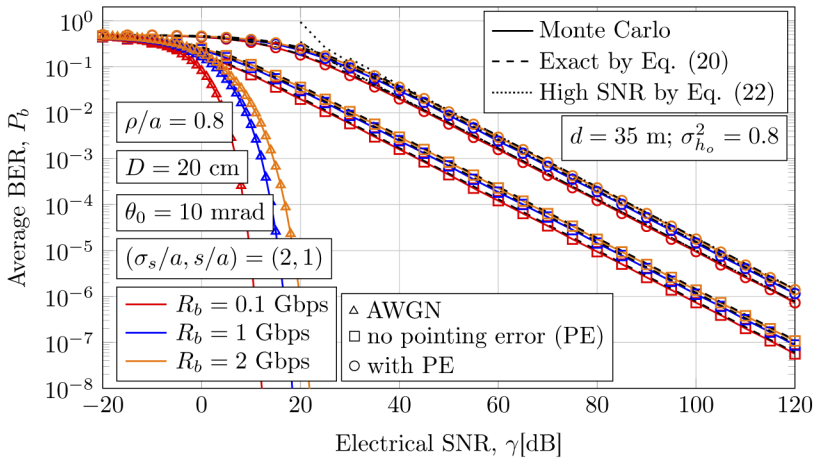

Fig. 3. Average BER performance for coastal water over salinity-induced oceanic turbulence in the presence of angular pointing errors when a receiver aperture diameter of $D = 20$ cm and a value of FOV= 180° are considered. These BER results correspond to a UOWC system using NRZ OOK modulation for different values of the data rate of $R_b = \{0.1, 1, 2\}$ Gbps.

dispersion is taken into account. From Eq. (22), the OPP[dB] is readily derived as

$$\text{OPP[dB]} = \frac{20}{\beta_1} \log\left(\frac{1}{2^M} \sum_{a_k} (1 - X_k)^{-\beta_1}\right). \tag{24}$$

In Fig. 4, the above expression is plotted for coastal water as a function of the data rate, R_b (Gbps), for different UOWC link distances of $d = \{15, 25, 35\}$ m. The rest of UOWC system parameters used in this figure are the same ones as in Fig. 3. It is confirmed that as the data rate increases, the optical power penalty induced by ISI notably increases. When the UOWC link distance is not too long, it may be feasible to increase the transmitted optical power to reduce

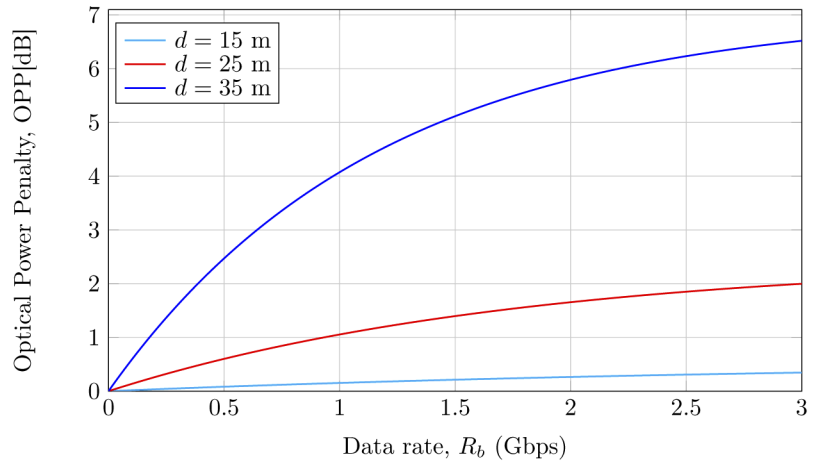

Fig. 4. OPP[dB] as a function of the data rate, R_b (Gbps), for coastal water when a receiver aperture diameter of $D = 20$ cm and a value of FOV= 180° are considered. The same set of UOWC system parameters as in Fig. 3 is used.

Optics EXPRESS

the effect of ISI under eye-safety regulation. In another way, for longer distances, equalization techniques are needed. In short, the UOWC channel is far away from being modeled as a flat one where ISI does not happen. Finally, as we can see in Fig. 3, the optical power penalty obtained for a value of data rate of $R_b = 0.1$ Gbps is ~ 0.7 dB since the effect of scattering is not so relevant at this transmission rate. However, when scattering becomes important, optical power penalties of ~ 4.25 dB and ~ 5.55 dB are obtained for values of data rate of $R_b = 1$ Gbps and $R_b = 2$ Gbps, respectively.

6. Conclusion

In this paper, the BER performance of UOWC systems has been carefully analyzed in the presence of absorption and scattering over salinity-induced oceanic turbulence channels with angular pointing errors. The developed BER closed-form expression, which is valid over a wide range of SNR, has been verified by Monte Carlo simulation results for clear ocean and coastal waters.

In the light of the results presented here, it is been demonstrated that the use of a laser source in the blue-green band allows to deploy longer UOWC point-to-point links for ocean observation purposes. On the one hand, the performance of such systems has been analyzed in detail by modeling firstly the attenuation due to geometric spread in the presence of scattering and, hence, estimating the true received power. Because of scattering, the optical beam arriving at the receiver plane is broadened even more, providing it with a natural mechanism to combat such a fading effect at the expense of a higher attenuation since it reduces the power captured on a fixed-size receiver. Our findings suggest that UOWC systems are less sensitive to angular pointing errors due to jitter. Furthermore, this sensitivity decreases as the water type becomes increasingly turbid. It is proved that that the effect of scattering cannot be ignored when modeling pointing errors in UOWC systems. The impact of increasing the data rate of the system has also been analyzed by computing the optical power penalty induced by ISI, showing that the underwater channel is far away being modeled as a flat one where ISI does not take place. Finally, we conclude that the results presented here can be considered of great relevance for communication purposes.

Beyond the work conducted here, there are other link configurations such as non-line-of-sight that allows to deploy robust data links with no need for perfect alignment, as well as assuming solar radiance penetration that should be investigated. In order to mitigate the effect of ISI caused by temporal dispersion, advanced equalization techniques should be also proposed. Future work in performance analysis of UOWC systems should concentrate on filling this gap.

Appendix A: Scintillation index

In order to analyze the BER performance of realistic UOWC scenarios, it is convenient to derive the corresponding expression of the scintillation index as a function of distance to determine the onset of strong fluctuations as well as to know which values of the scintillation index are valid for salinity-induced oceanic turbulence. As described in [51], assuming plane- and spherical-wave propagation through seawater, the scintillation index reduces to

$$\sigma_{h_o}^2(d) = 8\pi k^2 d \int_0^1 \int_0^\infty \kappa \Phi_n(\kappa) \left\{ 1 - \cos\left(\frac{d\kappa^2}{k} \xi \left(1 - (1-\Theta)\xi \right) \right) \right\} d\kappa d\xi, \tag{25}$$

where k is the wavenumber, and $\Phi_n(\kappa)$ is the power spectrum of oceanic turbulence fluctuations. Note that $\Theta = 1$ for plane wave, and $\Theta = 0$ for spherical wave. Here, we use the Nikishov's power spectrum of oceanic turbulence that is based on a linear combination of three scalar spectra of the temperature, salinity, and coupling fluctuations [49]. This model was obtained under assumptions that isotropic and homogeneous oceanic waters with respect to temperature and

Optics EXPRESS

salinity, and it is given by

$$\Phi_n(\kappa) = 0.388 \times 10^{-8} \epsilon^{-1/3} \kappa^{-11/3} \left[1 + 2.35(\kappa\eta)^{2/3}\right] \frac{\chi_T}{\omega^2} \left(\omega^2 e^{-A_T \delta} + e^{-A_s \delta} - 2\omega e^{-A_{TS} \delta}\right), \quad (26)$$

where ϵ represents the rate of dissipation of turbulent kinetic energy per unit mass of fluid, varying in the range of $10^{-2} - 10^{-8}$ m^2/s^3, $\eta = 10^{-3}$ m is the Kolmogorov microscale, χ_T is the rate of dissipation of mean-square temperature, varying in the range of $10^{-4} - 10^{-10}$ K^2/s, and ω is a unitless parameter that plays an important role in oceanic turbulence since it represents the relative strength of temperature and salinity fluctuations, taking values between -5 and 0. Oceanic turbulence is controlled by salinity when ω takes values nearby 0, and it is controlled by temperature when ω takes values nearby -5 [49,50]. Unfortunately, Eq. (25) cannot be expressed in closed-form. In practice, it is useful to derive a simple analytic approximation for the scintillation index. Thus, the scintillation index is estimated as

$$\sigma_{h_o}^2(d) \simeq \lambda_1 d^2 + \lambda_2 d + \lambda_3, \quad d \leq 100 \text{ m} \quad (27)$$

where λ_1, λ_2, and λ_3 are the parameters to be solved via curve fitting approach as summarized in Table 3. In Fig. 5, $\sigma_{h_o}^2(d)$ is depicted for different values of w when plane and spherical waves are considered. It can be observed that the above approximation matches very well with Eq. (25). This approximation achieves a value of coefficient of determination R-square (R^2) of 0.999.

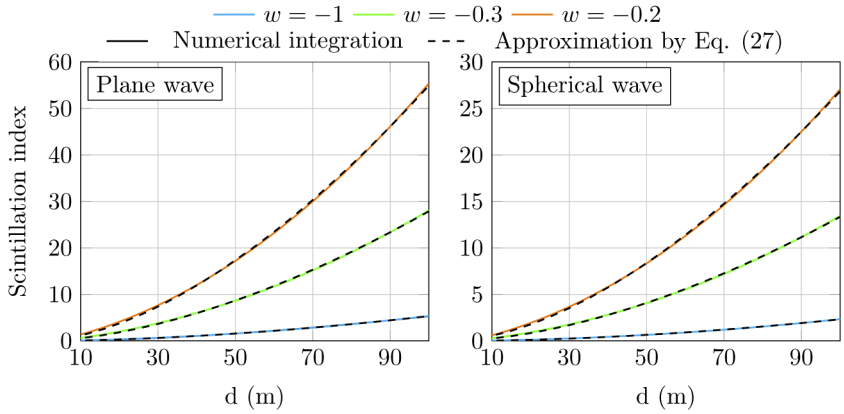

Fig. 5. Scintillation index for plane and spherical waves as a function of distance when different values of w are considered. Eq. (25) is solved numerically and is plotted by using solid curve, and Eq. (27) is plotted by using dashed curve. The rest of assumed values are $\epsilon = 10^{-5} m^2/s^3$, and $\chi_T = 10^{-7} K^2/s$.

Table 3. Scintillation index parameters.

Plane wave					Spherical wave				
w	λ_1	λ_2	λ_3	R^2	w	λ_1	λ_2	λ_3	R^2
-1	0.000536	0.00507	-0.013	0.999	-1	0.000204	0.00301	-0.0206	0.999
-0.3	0.00265	0.0436	-0.085	0.999	-0.3	0.00102	0.033	-0.158	0.999
-0.2	0.00535	0.0858	-0.114	0.999	-0.2	0.002	0.0732	-0.335	0.999

Appendix B: Geometric loss modeling

The attenuation due to geometric spread that a laser beam experiences when propagating through seawater is modeled analytically. For that, we need to compute the off-axis received power for

Optics EXPRESS

a Gaussian beam whose center is distance r from a circular receiver aperture of radius a. For non-dispersive channels, the attenuation due to geometric spread at the receiver was approximated in [37] as follows

$$h_p(r) \simeq A_0 \exp\left(-2r^2/\omega_{z_{eq}}^2\right), \tag{28}$$

where $A_0 = [\mathrm{erf}(v)]^2$ is the fraction of the collected power at $r = 0$ with $v = \sqrt{\pi}a/\sqrt{2}\omega_z$, $\omega_{z_{eq}}^2 = \omega_z^2\sqrt{\pi}\mathrm{erf}(v)/2v\exp(-v^2)$ is the equivalent beamwidth, $\omega_z = \theta_0 \cdot d$ is the beamwidth at the receiver plane, θ_0 is the divergence at $1/e$, and d is the link distance. In order to include the effect of angular misalignment, i.e. when the optical beam is non-orthogonal with respect to the photodetector plane, an extension of this geometric loss modeling was presented in [35] where the parameters A_0 and $\omega_{z_{eq}}^2$ were redefined through $v = \sqrt{\pi}\sqrt{a\rho}/\sqrt{2}\omega_z$ with $\rho = a\cos\theta\cos\phi$ being the parameter that determines the power reduction due to an angular misalignment. However, this model cannot be used in its current form since it does not include the effect of scattering. Due to the difficulty in solving analytically the radiative transfer equation (RTE) to take scattering into account, we compute the true received power numerically via Monte Carlo methods, as described in [7]. According to our simulations, the beam profile at the receiver plane is still Gaussian in nature for clear ocean and coastal waters, but it is required to include two degrees of freedom k_1 and k_2 due to scattering as

$$h_{ap}(r) \simeq k_1 A_0 \exp\left(-2r^2/\omega_{z_{eq}}^2\right), \tag{29a}$$

$$\omega_z(k_2) \simeq k_2 \cdot \theta_0 \cdot d, \tag{29b}$$

where k_1 and k_2 are the coefficients that are obtained via data fitting to simulation data to model the increase in beam spreading due to scattering. As we can observe from the above model, k_1 is a scale parameter, and k_2 is the parameter that models the beamwidth expansion, taking larger values as scattering becomes significant. In Fig. 6, the off-axis received power is plotted as a function of the horizontal radial displacement of the receiver for clear ocean and coastal waters by considering a laser beam with a divergence angle of 10 mrad. The results of geometric loss obtained via Monte Carlo simulations are displayed using solid line, and the results obtained analytically via Eq. (29) are displayed in dashed line. As can be seen in Table 4, a larger beamwidth due to scattering is derived in coastal water in comparison with clear ocean water. In general, while a higher geometric loss is obtained as the UOWC link distance increases, a higher robustness is achieved because of the beam expansion. Finally, we calculate the coefficient of determination R^2 of k_1 and k_2, obtaining always a value above 0.98, as outlined in Table 4.

Table 4. Geometric loss parameters.

Clear ocean water					Coastal water				
d (m)	k_1	k_2	ω_z/a	R^2	d (m)	k_1	k_2	ω_z/a	R^2
20	1.13	1.54	3.08	0.999	15	1.71	1.97	2.95	0.998
30	1.19	1.54	4.62	0.999	20	2.07	2.03	4.06	0.999
40	1.26	1.54	6.16	0.999	25	2.75	2.16	5.4	0.999
50	1.31	1.54	7.7	0.999	30	4.48	2.49	7.47	0.997
60	1.39	1.54	9.24	0.997	35	6.96	2.66	9.31	0.987

Optics EXPRESS

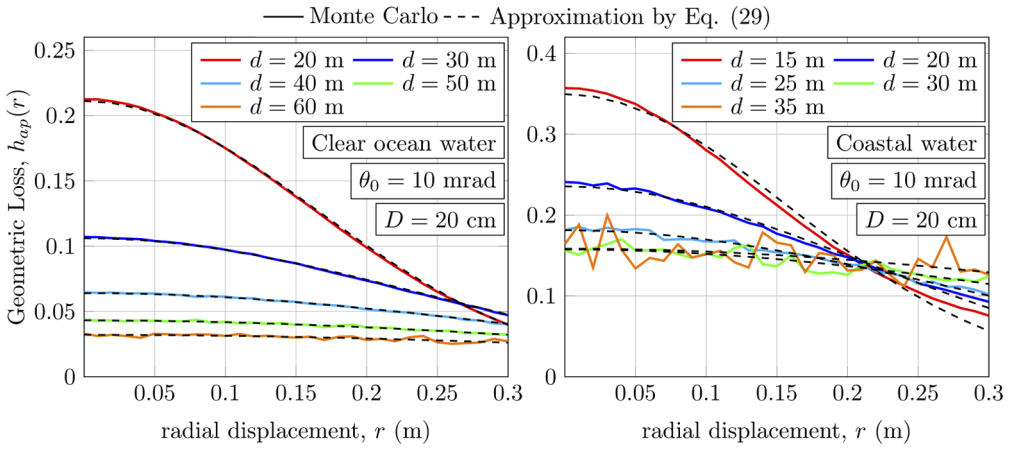

Fig. 6. $h_{ap}(r)$ as a function of the horizontal displacement r for clear ocean and coastal waters when a receiver aperture diameter of $D = 20$ cm and a value of FOV= 180° are considered when the divergence angle is set to $\theta_0 = 10$ mrad

Funding

Spanish MICINN Project (PID2019-107792GB-I00); Programa Operativo I+D+i FEDER Andalucia 2014-2020 (UMA18-FEDERJA-099, P18-RTJ-3343).

Disclosures

The authors declare no conflicts of interest.

References

1. X. Sun, C. H. Kang, M. Kong, O. Alkhazragi, Y. Guo, M. Ouhssain, Y. Weng, B. H. Jones, T. K. Ng, and B. S. Ooi, "A review on practical considerations and solutions in underwater wireless optical communication," J. Lightwave Technol. **38**(2), 421–431 (2020).
2. Z. Zeng, S. Fu, H. Zhang, Y. Dong, and J. Cheng, "A survey of underwater optical wireless communications," IEEE Commun. Surv. Tutorials **19**(1), 204–238 (2017).
3. C. D. Mobley, *Light and water: radiative transfer in natural waters* (Academic, 1994).
4. C. Gabriel, M.-A. Khalighi, S. Bourennane, P. Léon, and V. Rigaud, "Monte-Carlo-based channel characterization for underwater optical communication systems," J. Opt. Commun. Netw. **5**(1), 1–12 (2013).
5. S. Tang, Y. Dong, and X. Zhang, "Impulse response modeling for underwater wireless optical communication links," IEEE Transactions on Communications **62**(1), 226–234 (2014).
6. Y. Li, M. S. Leeson, and X. Li, "Impulse response modeling for underwater optical wireless channels," Appl. Opt. **57**(17), 4815–4823 (2018).
7. R. Boluda-Ruiz, P. Rico-Pinazo, B. Castillo-Vazquez, A. Garcia-Zambrana, and K. Qaraqe, "Impulse Response Modeling of Underwater Optical Scattering Channels for Wireless Communication," IEEE Photonics J. **12**(4), 1–14 (2020).
8. Y. Liu, J. Che, H. Xu, and C. Cao, "Adaptive attitude control of autonomous underwater vehicles using back-stepping," in *Proceedings of the 10th International Conference on Underwater Networks & Systems*, (2015), pp. 1–2.
9. J. Sakiyama and N. Motoi, "Position and attitude control method using disturbance observer for station keeping in underwater vehicle," in *IECON 2018-44th Annual Conference of the IEEE Industrial Electronics Society*, (IEEE, 2018), pp. 5469–5474.
10. U. Ansari and A. H. Bajodah, "Autonomous underwater vehicles attitude control using neuro-adaptive generalized dynamic inversion," IFAC-PapersOnLine **52**(29), 103–109 (2019).
11. S. A. Thorpe, *The turbulent ocean* (Cambridge University, 2005).
12. Y. Dong, S. Tang, and X. Zhang, "Effect of random sea surface on downlink underwater wireless optical communications," IEEE Commun. Lett. **17**(11), 2164–2167 (2013).
13. C. Gabriel, M.-A. Khalighi, S. Bourennane, P. Léon, and V. Rigaud, "Misalignment considerations in point-to-point underwater wireless optical links," in *2013 MTS/IEEE OCEANS-Bergen*, (IEEE, 2013), pp. 1–5.

Optics EXPRESS

14. W. Cox and J. Muth, "Simulating channel losses in an underwater optical communication system," J. Opt. Soc. Am. A **31**(5), 920–934 (2014).
15. R. A. Khalil, M. I. Babar, N. Saeed, T. Jan, and H.-S. Cho, "Effect of link misalignment in the optical-Internet of underwater things," Electronics **9**(4), 646 (2020).
16. W. Liu, Z. Xu, and L. Yang, "SIMO detection schemes for underwater optical wireless communication under turbulence," Photonics Res. **3**(3), 48–53 (2015).
17. M. V. Jamali, A. Chizari, and J. A. Salehi, "Performance analysis of multi-hop underwater wireless optical communication systems," IEEE Photonics Technol. Lett. **29**(5), 462–465 (2017).
18. M. V. Jamali, P. Nabavi, and J. A. Salehi, "MIMO underwater visible light communications: Comprehensive channel study, performance analysis, and multiple-symbol detection," IEEE Trans. Veh. Technol. **67**(9), 8223–8237 (2018).
19. N. Anous, M. Abdallah, M. Uysal, and K. Qaraqe, "Performance evaluation of LOS and NLOS vertical inhomogeneous links in underwater visible light communications," IEEE Access **6**, 22408–22420 (2018).
20. Y. Baykal, "Bit error rate of pulse position modulated optical wireless communication links in oceanic turbulence," J. Opt. Soc. Am. A **35**(9), 1627–1632 (2018).
21. A. Jurado-Navas, N. G. Serrato, J. Garrido-Balsells, and M. Castillo-Vázquez, "Error probability analysis of OOK and variable weight MPPM coding schemes for underwater optical communication systems affected by salinity turbulence," OSA Continuum **1**(4), 1131–1143 (2018).
22. A. Jurado-Navas, J. M. Garrido-Balsells, M. Castillo-Vazquez, A. García-Zambrana, and A. Puerta-Notario, "Converging underwater and FSO ground communication links," in *2019 Optical Fiber Communications Conference and Exhibition (OFC)*, (IEEE, 20191–3
23. M. C. Gökçe, Y. Baykal, and Y. Ata, "Binary phase shift keying-subcarrier intensity modulation performance in weak oceanic turbulence," Phys. Commun. **37**, 100904 (2019).
24. H. Jiang, H. Qiu, N. He, W. Popoola, Z. Ahmad, and S. Rajbhandari, "Performance of spatial diversity DCO-OFDM in a weak turbulence underwater visible light communication channel," J. Lightwave Technol. **38**(8), 2271–2277 (2020).
25. G. Xu and J. Lai, "Average capacity analysis of the underwater optical plane wave over anisotropic moderate-to-strong oceanic turbulence channels with the Málaga fading model," Opt. Express **28**(16), 24056–24068 (2020).
26. Y. Li, Y. Zhang, and Y. Zhu, "Capacity of underwater wireless optical links with pointing errors," Opt. Commun. **446**, 16–22 (2019).
27. M. Elamassie and M. Uysal, "Vertical underwater VLC links over cascaded gamma-gamma turbulence channels with pointing errors," in *2019 IEEE International Black Sea Conference on Communications and Networking (BlackSeaCom)*, (IEEE, 2019), pp. 1–5.
28. R. P. Naik, U. S. Acharya, and P. Krishnan, "Cooperative RF-UWOC link performance over hyperbolic tangent log-normal distribution channel with pointing errors," Opt. Commun. **469**, 125774 (2020).
29. H. M. Oubei, E. Zedini, R. T. ElAfandy, A. Kammoun, T. K. Ng, M.-S. Alouini, and B. S. Ooi, "Efficient Weibull channel model for salinity induced turbulent underwater wireless optical communications," in *2017 Opto-Electronics and Communications Conference (OECC) and Photonics Global Conference (PGC)* (IEEE, 2017), pp. 1–2.
30. M. V. Jamali, A. Mirani, A. Parsay, B. Abolhassani, P. Nabavi, A. Chizari, P. Khorramshahi, S. Abdollahramezani, and J. A. Salehi, "Statistical studies of fading in underwater wireless optical channels in the presence of air bubble, temperature, and salinity random variations," IEEE Trans. Commun. Technol. **66**(10), 1 (2018).
31. I. Toselli and S. Gladysz, "Improving system performance by using adaptive optics and aperture averaging for laser communications in oceanic turbulence," Opt. Express **28**(12), 17347–17361 (2020).
32. E. A. Lee and D. G. Messerschmitt, *Digital communication* (Kluwer Academic Publishers, 1994).
33. A. García-Zambrana, C. Castillo-Vázquez, and B. Castillo-Vázquez, "Outage performance of MIMO FSO links over strong turbulence and misalignment fading channels," Opt. Express **19**(14), 13480–13496 (2011).
34. I. S. Gradshteyn and I. M. Ryzhik, *Table of integrals, series and products*, 7th ed. (Academic Press Inc., 2007).
35. R. Boluda-Ruiz, A. García-Zambrana, B. Castillo-Vázquez, and K. Qaraqe, "Secure communication for FSO links in the presence of eavesdropper with generic location and orientation," Opt. Express **27**(23), 34211–34229 (2019).
36. M. Najafi, H. Ajam, V. Jamali, P. D. Diamantoulakis, G. K. Karagiannidis, and R. Schober, "Statistical modeling of the FSO fronthaul channel for UAV-based communications," IEEE Trans. Commun. Technol. **68**(6), 3720–3736 (2020).
37. A. A. Farid and S. Hranilovic, "Outage capacity optimization for free-space optical links with pointing errors," J. Lightwave Technol. **25**(7), 1702–1710 (2007).
38. P. Beckmann, "Statistical distribution of the amplitude and phase of a multiply scattered field," J. Res. NBS D **66D**, 231–240 (1962).
39. R. Boluda-Ruiz, A. García-Zambrana, C. Castillo-Vázquez, and B. Castillo-Vázquez, "Novel approximation of misalignment fading modeled by Beckmann distribution on free-space optical links," Opt. Express **24**(20), 22635–22649 (2016).
40. M. Abramowitz and I. A. Stegun, *Handbook of mathematical functions with formulas, graphs, and mathematical tables*, 9th ed (Dover, New York, 1970).
41. Wolfram Research, Inc., The Wolfram functions site. [Online]. Available: http://functions.wolfram.com.
42. A. A. Kilbas, *H-transforms: Theory and Applications* (CRC, 2004).

Optics EXPRESS

43. R. Boluda-Ruiz, A. García-Zambrana, C. Castillo-Vázquez, B. Castillo-Vázquez, and S. Hranilovic, "Outage performance of exponentiated Weibull FSO links under generalized pointing errors," J. Lightwave Technol. **35**(9), 1605–1613 (2017).
44. A. P. Prudnikov, Y. A. Brychkov, and O. I. Marichev, *Integrals and series Volume 2: Special Functions*, vol. 2, 1st ed (Gordon and Breach Science Publishers, 1986).
45. C. Shen, Y. Guo, X. Sun, G. Liu, K.-T. Ho, T. K. Ng, M.-S. Alouini, and B. S. Ooi, "Going beyond 10-meter, Gbit/s underwater optical wireless communication links based on visible lasers," in *2017 opto-electronics and communications conference (OECC) and photonics global conference (PGC)*, (IEEE, 2017), pp. 1–3.
46. X. Liu, S. Yi, X. Zhou, Z. Fang, Z.-J. Qiu, L. Hu, C. Cong, L. Zheng, R. Liu, and P. Tian, "34.5 m underwater optical wireless communication with 2.70 Gbps data rate based on a green laser diode with NRZ-OOK modulation," Opt. Express **25**(22), 27937–27947 (2017).
47. C. Lu, J. Wang, S. Li, and Z. Xu, "60m/2.5 Gbps underwater optical wireless communication with nrz-ook modulation and digital nonlinear equalization," in *2019 Conference on Lasers and Electro-Optics (CLEO)*, (2019), pp. 1–2.
48. "The Sonardyne site: Bluecomm underwater optical communications. Sonardyne International ltd,". http://www.sonardyne.com/.
49. V. Nikishov and V. Nikishov, "Spectrum of turbulent fluctuations of the sea-water refraction index," Int. J. Fluid Mech. Res. **27**(1), 82–98 (2000).
50. O. Korotkova, N. Farwell, and E. Shchepakina, "Light scintillation in oceanic turbulence," Waves in Random and Complex Media **22**(2), 260–266 (2012).
51. L. C. Andrews and R. L. Phillips, *Laser beam propagation through random media*, vol. 1 (SPIE, 2005).